[CANCER RESEARCH 63, 5970–5977, September 15, 2003]

Multicellular Resistance to Tirapazamine Is Due to Restricted Extravascular Transport: A Pharmacokinetic/Pharmacodynamic Study in HT29 Multicellular Layer Cultures[1]

Kevin O. Hicks,[2] Frederik B. Pruijn, Joanna R. Sturman, William A. Denny, and William R. Wilson

Auckland Cancer Society Research Centre, The University of Auckland, Private Bag 92019, Auckland, New Zealand

ABSTRACT

In common with other bioreductive drugs, metabolic reduction is required for activation of the benzotriazine-di-*N*-oxide tirapazamine (TPZ) in hypoxic regions of tumors. This same metabolism also consumes the drug as it diffuses, impeding its penetration into hypoxic tissue. In this study, we develop a pharmacokinetic (PK)/pharmacodynamic (PD) model for TPZ that explicitly includes its diffusion characteristics as measured in multicellular layer (MCL) cultures of HT29 colon carcinoma cells. The kinetics of TPZ metabolism to its mono-*N*-oxide derivative SR 4317, determined by high-performance liquid chromatography using anoxic HT29 single cell suspensions, demonstrated both a first order and saturable (K_m = 3.6 μM) component. Cell killing, assessed by clonogenic assay under the same conditions, demonstrated an approximately quadratic concentration dependence and linear time dependence. TPZ transport through MCLs, determined under hyperoxic conditions (95% O_2) to suppress reductive metabolism, provided a concentration-independent diffusion coefficient of 0.40 × 10^{-6} cm^2s^{-1}. Under anoxia, this transport was strongly suppressed and was well predicted by the single cell metabolism parameters (scaled to the cell density in MCLs). These PK (transport) and PD (cytotoxicity) parameters were used to calculate cell killing as a function of distance in anoxic HT29 MCLs after the addition of TPZ to both sides of the MCL. The predicted average cell kill was in good agreement with measured values, which showed much less killing than for single cell suspensions under the same conditions. The success of this PK/PD model in predicting response in MCL shows that inefficient transport, rather than changes in intrinsic sensitivity, is responsible for TPZ resistance in these three-dimensional cell cultures and suggests that optimization of transport properties is a high priority in developing second-generation TPZ analogues.

INTRODUCTION

Many studies have shown that tumor cells in three-dimensional contact with each other or with extracellular matrix, whether in tumors or multicellular spheroids in culture, are more resistant to ionizing radiation and cytotoxic drugs than are cells in monolayer culture (1–3). The causes of this "multicellular resistance" are interrelated and multifactorial (4–6), including adhesion-dependent changes in cell cycle progression (7, 8) and apoptosis (9, 10), changes in cell shape, gap junctional communication, chromatin packing, and expression of growth factors and other gene products (4, 6). In addition, the microenvironment in solid tumors, notably hypoxia and low extracellular pH, may lead to resistance (11) either directly (as for ionizing radiation) or indirectly through cytokinetic changes or expression of stress proteins including P-glycoprotein (12). These factors can all be considered as PD[3] differences between cells in a tissue-like microenvironment *versus* low-density cultures. In addition, for chemotherapy drugs, PK limitations because of inefficient diffusion through tissue may contribute to multicellular resistance and may be an important (if poorly understood) component of "intrinsic" chemoresistance in the treatment of solid tumors (13, 14). Despite this, effect compartment measurements or models are rarely used to assess the relative contribution of the PK and PD components of multicellular drug resistance.

A recent initiative in chemotherapy has been the development of drugs that exploit features of the tumor microenvironment (15), as shown by the benzotriazine-di-*N*-oxide TPZ, which is selectively cytotoxic to hypoxic cells (16, 17) and is currently in clinical trial (18). The PK (penetration) problem is especially critical for hypoxic cytotoxins; not only are their target cells distant from functional blood vessels, necessitating long extravascular diffusion distances, but these "bioreductive" drugs are activated by metabolic reduction via oxygen-inhibited pathways as shown for TPZ in Fig. 1. This necessarily consumes the drug as it diffuses, potentially compromising its extravascular transport. Making multicellular spheroids more hypoxic has been shown to cause apparent resistance of the innermost cells to TPZ, consistent with such an extravascular transport problem (19). In addition, studies with the MCL model, in which tumor cells are grown on a permeable support to form multicellular layers, have demonstrated more directly that TPZ transport is impeded by rapid drug metabolism under hypoxic conditions (20–22). The latter studies included mathematical simulations that suggested the penetration problem to be severe enough to confer apparent resistance, although this conclusion depended on PD parameters (cytotoxicity) measured in other cell lines and was not tested experimentally. Thus, the two types of observations in the literature (resistance in spheroids, impeded transport in MCLs) have not been combined in a way that makes it possible to assess quantitatively whether the PK (penetration) problem is the main contributor to the observed PD (resistance) problem with TPZ. This is the main objective of the present study.

To achieve this objective, we develop a detailed PK/PD model for cell killing by TPZ as a function of diffusion distance in MCLs. The MCLs are grown from HT29 colon carcinoma cells, and all of the parameters of the model are determined using this cell line. The PK parameters include the diffusion coefficient of TPZ in HT29 MCLs (D_{MCL}) and kinetics of its metabolism under anoxia (determined in single cell suspensions). The PD parameters describe the relationship between exposure and cell killing, also determined in single cell suspensions. The predictions of the PK/PD model are tested against measured cell killing in HT29 MCLs. The results show that the extravascular transport problem can entirely account for the apparent difference in TPZ sensitivity between single cells and cells in three-dimensional contact and demonstrate that improving transport parameters is an important goal in developing a second-generation TPZ analogue.

Received 11/18/02; revised 5/15/03; accepted 7/8/03.

The costs of publication of this article were defrayed in part by the payment of page charges. This article must therefore be hereby marked *advertisement* in accordance with 18 U.S.C. Section 1734 solely to indicate this fact.

[1] Supported by NIH National Cancer Institute Grant PO1-CA82566 and by the Health Research Council of New Zealand.

[2] To whom requests for reprints should be addressed, at Auckland Cancer Society Research Centre, The University of Auckland, Private Bag 92019, Auckland, New Zealand. Phone: 64-9-3737-599, ext. 86939; Fax: 64-9-3737-571; E-mail: k.hicks@auckland.ac.nz.

[3] The abbreviations used are: PD, pharmacodynamic; HPLC, high-performance liquid chromatography; MCL, multicellular layer; PK, pharmacokinetic; TPZ, tirapazamine.

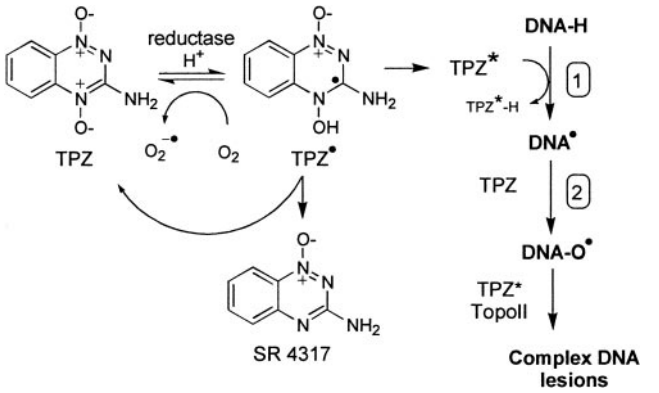

Fig. 1. Mechanism of activation of TPZ, via reduction to an oxygen-sensitive radical (TPZ•), which decays to form a DNA-oxidizing radical (TPZ*) such as the hydroxyl radical (42) or benzotriazyl radical (43). The resulting DNA radicals are oxidized further by a second molecule of TPZ (step 2). Interaction with additional TPZ radicals and/or TopoIIα generates complex DNA lesions including double-strand breaks.

MATERIALS AND METHODS

Chemicals and Radiochemicals. TPZ was synthesized using a published method (23), dissolved in DMSO at 300 mM, and diluted at least 100-fold into culture medium. [*U*-^{14}C]mannitol (8.55 GBq/mmol) was purchased from ICN Biomedicals Inc. (Irvine, CA), and [^{14}C]urea (2.11GBq/mmol) and [^{3}H]$_2$O (185 GBq/μl) were from Amersham Pharmacia Biotech (Sydney, Australia). Radiochemicals were dissolved in 50% ethanol, stored at −20°C, and diluted at least 100-fold into culture medium for experiments.

Growth of Monolayers, MCL, and Spheroids. HT29 human colon carcinoma cells (obtained from Dr. David Ross, University of Colorado, Denver, CO) were passaged in αMEM (Life Technologies, Inc., Grand Island, NY) with 5% fetal bovine serum (Life Technologies, Inc., Auckland, New Zealand) without antibiotics and were confirmed to be free of *Mycoplasma* using a PCR-ELISA assay (Roche Diagnositics GmbH, Mannheim, Germany). MCLs (Fig. 2) were grown on collagen-coated Teflon supports (Millicell-CM cell culture inserts; Millipore Corp., Bedford, MA) as described previously (24, 25) by seeding 10^6 cells. After allowing cells to attach for 6 h, the inserts were submerged in stirred αMEM containing 10% fetal bovine serum, 2 mM L-glutamine, penicillin (100 units/ml), and streptomycin (100 μg/ml), and grown for an additional 3 days. This medium was used for all subsequent experiments. Multicellular spheroids were grown in the same medium by seeding 10^5 cells into bacteriological P100 Petri dishes; 7 days later, they were transferred to Bellco spinner flasks (Invitrogen, CA) and grown for an additional 8 days with medium replacement every 3 days. Single cell suspensions were prepared by enzymatic dissociation of MCL or spheroids in 0.07% trypsin (Difco Laboratories, Detroit, MI) in saline containing trisodium citrate (14 mM, pH 7.6) for 10 min.

MCL Histology and Thickness Measurements. MCLs were fixed in 2% neutral-buffered formalin at 4°C for 48 h and then transferred to PBS [137 mM NaCl, 2.68 mM KCl, 1.47 mM KH_2PO_4, and 8.10 mM Na_2HPO_4 (pH 7.4)] at 4°C. Paraffin sections were prepared by cutting the support membrane and MCL from the insert with a scalpel, placing between embedding sponges, and transferring to cassettes for automated histological processing (26). Sections were cut at a thickness of 4 μm and stained with H&E. Frozen sections were prepared after fixing as above by embedding in Tissue Tek OCT (Miles Inc., Elkart, IN) and freezing rapidly with liquid nitrogen-cooled isopentane. Transverse (10 μm) sections were cut at intervals of 1 mm and air dried on silane-coated glass slides. MCL thickness was determined at intervals of 40 μm along each section using a charge-coupled device (CCD) camera attached to a Nikon Optiphot microscope, calibrating against the known thickness of the Teflon membrane (30 μm; Ref. 24).

Uptake, Metabolism, and Cytotoxicity in Single-Cell Suspensions. Stirred suspensions (0.5–5 × 10^6 cells/ml) derived from HT29 spheroids were incubated with TPZ at a range of initial concentrations under 20% O_2 or anoxia (<200 ppm O_2, as confirmed with an Oxylite oxygen probe; Oxford Optronix, Oxford, United Kingdom). Suspensions were equilibrated with the appropriate gas phase for 1 h before the addition of drug. Cells and medium were separated by rapid centrifugation (16,000 × *g*, 1 min), followed by a brief second spin to remove medium from the walls of the tube. Concentrations of TPZ and its mono-*N*-oxide derivative SR 4317 were determined by HPLC of the extracellular medium and cell pellets (see below). Cell killing was determined by clonogenic assay of separate cell pellets in the same experiments; cells were washed by centrifugation in fresh medium, and serial dilutions were plated in Falcon P60 tissue culture dishes (Becton Dickinson Biosciences, Bedford, MA) at up to 10^5 cells/dish. Dishes were stained with methylene blue (2 g/liter in 50% ethanol) 14 days later, and colonies containing ≥50 cells were counted. The surviving fraction was determined as the ratio of plating efficiency of treated cells to that of controls (exposed to an equal concentration of DMSO) at the same time. Metabolism and survival data were fitted simultaneously to the model described in "Appendix I."

Analytical Methods. TPZ and SR 4317 in extracellular medium was assayed by HPLC after deproteinizing samples with 20 μl/ml of 70% (v/v) perchloric acid, centifugation, and adjustment of pH to 7 with 31.5 μl/ml of 50% (v/v) aqueous ammonia. In cell uptake experiments, the cell pellet was lyzed with 100 μl of ice-cold water, followed by deproteinization with 80% acetonitrile containing *N*,*N*-bis(2-chloroethyl)-*N*-methyl-*N*-(4-methyl-2-nitrobenzyl)ammonium chloride, as internal standard (27), evaporated to 50 μl and made up to 200 μl with mobile phase for HPLC injection. The HPLC system was a HP 1100 (Agilent, Palo Alto, CA) equipped with a diode-array detector and an Alltima C8 (150 × 2.1 mm, 5 μm; Alltech Associated Inc., Deerfield, IL) reverse phase column at a flow rate of 0.5 ml/min and an injection volume of 10–100 μl. The mobile phase comprised a gradient of acetronitrile in 0.45 M ammonium formate (pH 4.5). Absorbance was monitored at 462 nm for TPZ (to avoid a small coeluting peak at 13.3 min, which absorbs at the TPZ maximum of 266 nm) and 415 nm for SR4317 (retention time, 19.0 min). Standards at known concentrations were included in each experiment. The peak area was linearly related to the amount injected in the range 0.01–10 nmol ($r^2 > 0.999$), and recovery from medium was >95% for both analytes.

^{14}C and [^{3}H] activity was determined by scintillation counting in 5 ml of Emulsifier-Safe scintillant using a Packard Tricarb 1500 Liquid Scintillation Analyzer (Canberra Packard, Meriden, CT).

HT29 Cell Volume and Intracellular Volume Fraction in MCLs. Stirred suspensions of HT29 cells, dissociated from MCLs, were incubated at 5 × 10^6 cells/ml under the same gassing conditions as the metabolism and survival experiments. After the addition of [^{3}H]$_2$O and [^{14}C]mannitol to preequilibrated vials, samples of 0.5 ml were taken every 15 min for 1 h, and the extracellular medium and cell pellet [solubilized with 1 ml of Soluene-350 (Packard) at 60°C for 1 h] were assayed for [^{3}H] and ^{14}C activity by scintillation counting as above but using Hionic-Fluor (Packard) organic scintillant for the cell pellet. The intracellular water volume in the pellet was determined from the difference between the total and extracellular water volumes as estimated from the activities of the [^{3}H]$_2$O and [^{14}C]mannitol tracers, respectively. No time trend was observed, so all values were averaged. Intracellular volume fraction in HT29 MCLs was determined similarly, under the same conditions as flux experiments, after a 1-h equilibration after adding the tracers to both sides of the MCLs. Excess medium was aspirated, and the total [^{3}H] and ^{14}C activity in the MCL was determined after its removal and solubilization as above.

Diffusion of TPZ through MCLs (Flux Experiments). MCL experiments were performed in custom-built diffusion chambers (25) in which the MCL separates two well-stirred compartments, each containing 7 ml of medium under 5% CO_2 in 95% O_2 or 95% N_2, which maintained pH at 7.4 ± 0.1 throughout the experiments. MCLs were equilibrated in the diffusion chambers for 1 h at 37°C before removal of 130 μl from the donor compartment and its replacement with an equal volume of medium containing TPZ (final concentration, 1–100 μM) and [^{14}C]urea (internal standard; final concentration, 3 μM). Samples of 0.5 ml were taken from both compartments at intervals; 25 μl were

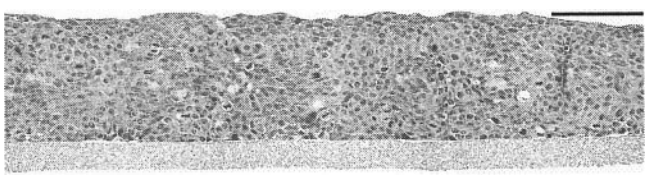

Fig. 2. H&E-stained paraffin section of an HT29 human colon carcinoma MCL grown submerged for 3 days. *Bar*, 100 μm.

used for scintillation counting, and the balance was stored at −80°C for HPLC. Similar experiments were performed using collagen-coated inserts without MCLs to check for chemical stability and to determine the effective diffusion coefficient of TPZ in the support membrane. Diffusion coefficients were determined from flux data by fitting the concentration-time profiles in both the donor and receiver compartment simultaneously, using the approach described in "Appendix II." The thickness of each MCL was determined from the flux of [^{14}C]urea, using the diffusion coefficient of this internal standard as determined separately in HT29 MCLs, in which thickness was measured by frozen section immediately after the experiment (see "Results").

Cytotoxicity of TPZ in Anoxic MCLs. MCL cytotoxicity studies were performed in the same apparatus as the transport studies. MCLs were equilibrated under anoxia for 2 h, during which time [^{14}C]urea flux was measured to determine the thickness of each MCL as above. TPZ was then introduced into both donor and receiver compartments (0, 50, 75, or 100 μM), and MCLs were incubated for an additional 1 or 2 h. Initial and final TPZ concentrations were measured by HPLC. After exposure, the MCLs were trypsinized and plated for clonogenic assay.

RESULTS

Cellular Uptake and Metabolism of TPZ. Cellular uptake and metabolism of TPZ was investigated by HPLC in stirred suspensions of HT29 cells obtained by trypsinizing multicellular spheroids. Concentrations of TPZ in extracellular medium and lyzed cell pellets were independent of concentration and constant with time under aerobic conditions between 1 and 4 h, with a ratio of intracellular:extracellular concentration (C_i/C_e) of (0.77 ± 0.10; n = 7). C_i/C_e was slightly lower (0.57 ± 0.06; n = 12) under anoxia, but the apparent decrease in uptake was shown to be an artifact caused by metabolism of TPZ to its mono-*N*-oxide metabolite (SR 4317) during preparation of cell pellets (data not shown). Under the same conditions, the more lipophilic metabolite SR 4317 showed slightly higher uptake factors (C_i/C_e *ca* 2.5 under both aerobic and anoxic conditions). These low uptake factors mean that >99% of the TPZ and SR 4317 is extracellular at the cell densities used ($\leq 5 \times 10^6$ cells/ml). Given that the mass balance was dominated by the extracellular compartment, it was appropriate to monitor overall metabolism by assaying the extracellular medium only.

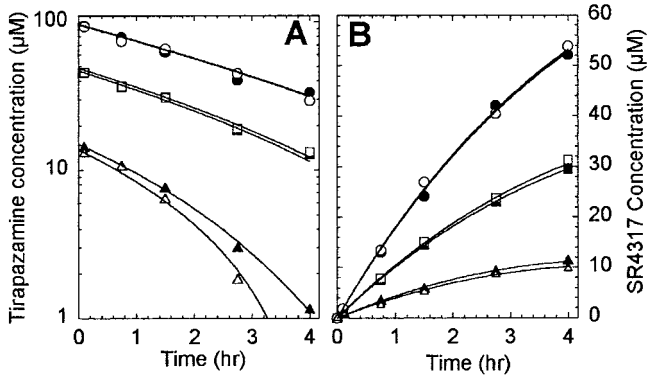

Fig. 3. A representative experiment investigating TPZ metabolism by HT29 cell suspensions (5×10^6/ml) under anoxia at a range of initial TPZ concentrations (○, ●: 100 μM; □, ■: 50 μM; ▲, △: 14 μM). *A*, TPZ loss. *B*, SR4317 production. The data were fitted to the metabolism model outlined in "Appendix I" (Eq. A2 and A3) by nonlinear regression.

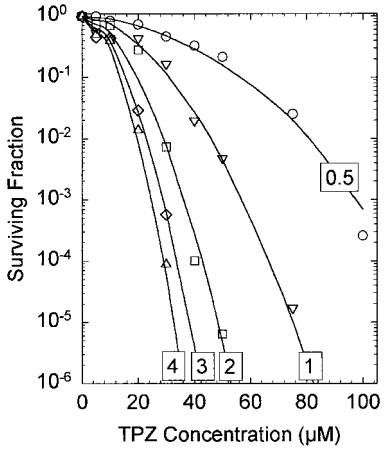

Fig. 4. Cytotoxicity of TPZ in anoxic HT29 cell suspensions (5×10^5 cells/ml) for the exposure times shown (h). *Lines* are nonlinear regression fits to the numerical solution of the PD model ("Appendix I," Eq. A4).

The kinetics of TPZ metabolism under anoxia was determined by following TPZ loss and SR 4317 formation at a range of cell densities and initial TPZ concentrations (10–150 μM), as shown for a typical experiment in Fig. 3. TPZ loss was first order at high concentrations, but faster relative metabolism was evident at <10 μM. No loss of TPZ was seen in anoxic culture medium without cells, even at low concentrations (data not shown). For each experiment, the TPZ and SR 4317 concentrations were simultaneously fitted to a metabolism model (see "Appendix I," Eq. A2) with first-order and saturable (Michaelis-Menten) terms as shown in Fig. 3. The estimated metabolism parameters were then averaged across experiments and used as initial parameter estimates to fit all data across all experiments simultaneously (28 concentration-time profiles), to give the values shown in Table 1.

Cytotoxicity of TPZ in Single-Cell Suspensions (PD Model). Cell killing was assessed by clonogenic assay over a similar range of cell densities (0.5–5 × 10^6 cells/ml) and initial TPZ concentrations (5–100 μM), often in the same experiments in which TPZ metabolism was determined; a representative data set is shown in Fig. 4. Anoxic cytotoxicity was greater for high than low TPZ concentrations at equivalent concentration (C) × time (T), as shown by the greater killing with 100 μM TPZ for 0.5 h than 50 μM for 1 h in Fig. 4. The C-T dependence was fitted well (Fig. 4, *lines*) by a PD model in which the rate of log cell killing is proportional to the product of the TPZ concentration and the rate of its metabolism (see "Appendix I"). At low cell density, when the TPZ concentration can be approximated as a constant, this model gives a log cell kill approximately proportional to exposure time and concentration squared (see "Appendix I").

TPZ Transport in HT29 MCLs. The above PK/PD model was determined for single cells dissociated enzymatically immediately

Table 1 *Parameters of the PK/PD model for TPZ metabolism and cytotoxicity in anoxic HT29 cell suspensions*

The model is described in "Appendix I."

Parameter	Units	Description	Mean ± SE (n)
f_m		SR 4317 yield as a fraction of TPZ metabolized	0.73 ± 0.08 (28 curves)
k_{met}	min^{-1}	First order rate constant for TPZ metabolism	0.78 ± 0.03 (28)[a]
V_{max}	$\mu M.min^{-1}$	Maximal rate for Michaelis-Menten component of TPZ metabolism	8.5 ± 2.2 (28)[a]
K_m	μM	Michaelis constant for TPZ metabolism	3.5 ± 3.5 (28)
α	μM^{-2}	Proportionality constant in PD model	(2.33 ± 0.05) × 10^{-5} (14 curves)
T_{lag}	min	Time lag to onset of killing in PD model	13.9 ± 2.9 (14)

[a] Normalized to intracellular density as described in "Appendix I."

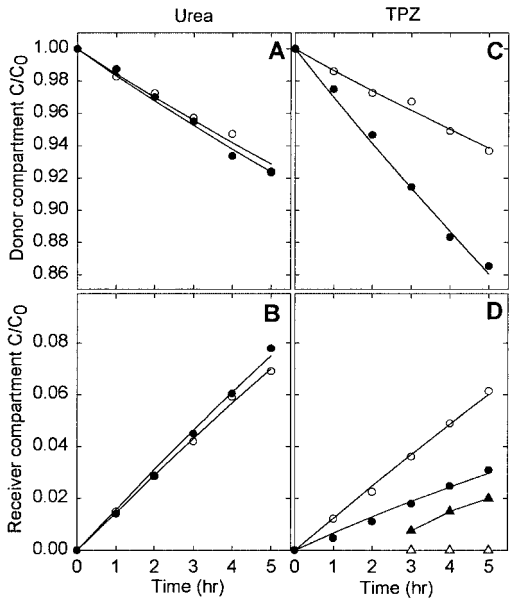

Fig. 5. TPZ diffusion through representative HT29 MCL under oxic (95% O_2, *open symbols*) and anoxic (*filled symbols*) conditions, respectively. *A* and *B*, [^{14}C]-urea internal standard. *Lines* are model fits, used to determine the effective thickness of the MCLs (146 μm for the oxic MCL; 137 μm for the anoxic MCL). *C* and *D*, TPZ diffusion (*circles*) through the same MCLs. *Lines* are model fits to the reaction-diffusion equation (see "Appendix II"). Concentrations of SR4317 in the receiver compartment are shown as *triangles*.

before exposure to TPZ. Whether it also applies to cells in a tissue-like environment was assessed by determining killing in intact HT29 MCLs, which were grown for 3 days after seeding with 10^6 cells to give densely cellular, uniform structures lacking central necrosis (Fig. 2). At this time, MCL thicknesses were approximately 140 μm. Previous studies have shown that transport of TPZ into hypoxic MCLs is significantly impeded by its bioreductive metabolism (20–22). Thus, prediction of PD response in MCLs requires information about the TPZ concentration-time profile as a function of distance into the MCL.

Diffusion coefficients were determined following the approach described previously for EMT6 and MGH-U1 MCLs (20), but using an apparatus that allowed measurement of TPZ concentrations on both sides of the MCL (22, 25); this more tightly constrains fitting of the data to the transport model (see "Appendix II"). Typical raw data are shown for TPZ and the internal standard, urea, in HT29 MCLs in Fig. 5. The key parameter values are reported in Table 2. First, the apparent diffusion coefficients of urea and TPZ were determined in the collagen-coated Teflon support membrane (D_s). Second, flux of urea through Teflon supports bearing MCLs of known thickness [197 $\pm$ 22 μm (mean $\pm$ SE) for six MCLs as determined by histology] was fitted to determine the diffusion coefficient for urea in HT29 MCLs (D_{MCL}). All these values were independent of O_2 concentration (data not shown). TPZ flux through MCLs was then investigated using 95% O_2 in the gas phase, which effectively suppressed bioreductive metabolism as shown by the TPZ mass balance and lack of formation of SR 4317 in Fig. 5. The data were well fitted as simple Fickian diffusion, with D_{MCL} as the sole fitted parameter, using the flux of the urea internal standard to estimate the thickness of each MCL. D_{MCL} for TPZ was independent of the initial TPZ concentration in the donor compartment over the range 1–90 μM (Fig. 6*A*), with a best estimate of $(0.40 \pm 0.01) \times 10^{-6}$ cm^{2}s^{-1} (Table 2). This was approximately 2-fold and 3-fold lower that the TPZ diffusion coefficients measured previously in V79 and MGH-U1 MCL (0.74 ± 0.03 and 1.3 ± 0.2 cm^{2}s^{-1}), respectively (20). Similar trends were seen in urea and sucrose diffusion coefficients determined in previous studies (20, 24) and probably reflects differences in extracellular space and tortuosity between MCL grown from different cell lines.

When the HT29 MCLs were anoxic, TPZ loss from the donor compartment was enhanced (Fig. 5*C*), and flux into the receiver compartment was suppressed, with accompanying formation of SR 4317 (Fig. 5*D*). These features, coupled with the lack of effect of anoxia on urea flux (Fig. 5, *A* and *B*), pointed to bioreductive metabolism in the MCL as the reason for impeded TPZ transport. We tested whether the decrease in TPZ flux could be quantitatively accounted for by the rate of TPZ metabolism observed in single cells above. This required scaling the single cell metabolism parameters to correct for the higher cell density in MCLs. We used [^{3}H]$_2$O and [^{14}C]mannitol as markers for total and extracellular water volumes, respectively, to determine the average intracellular water volume in cell pellets of

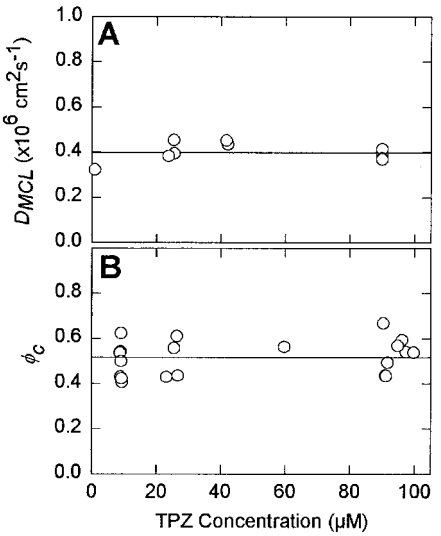

Fig. 6. Parameters of the model (see "Appendix II") describing transport of TPZ through HT29 MCLs, plotted against the initial TPZ concentration in the donor compartment. *A*, D_{MCL} of TPZ in oxic MCLs. *B*, estimated intracellular volume fraction in MCLs, ϕ_c, used to scale the single cell metabolism model (comprising a first order and Michaelis-Menten term; see "Appendix I") to the cell density in MCLs. The linear regressions for both D_{MCL} and ϕ_c show them to be concentration independent (slope not significantly different from zero; $P > 0.3$).

Table 2 *Parameters of the TPZ transport model for HT29 MCLs*

The model is described in "Appendix II." The other parameters of the transport model are the TPZ metabolism parameters, determined in single cell suspensions (Table 1) and scaled to the cell density in MCLs using ϕ_c.

Parameter	Units	Description	Value $\pm$ SE (n)
D_s Urea (M_r 60)	cm^{2}s^{-1} $\times$ 10^6	Diffusion coefficient for urea in Teflon support	2.08 $\pm$ 0.05 (19)
D_s TPZ (M_r 178)	cm^{2}s^{-1} $\times$ 10^6	Diffusion coefficient of TPZ in Teflon support	1.26 $\pm$ 0.04 (5)
D_{MCL} Urea	cm^{2}s^{-1} $\times$ 10^6	Diffusion coefficient of urea in HT29 MCL	0.450 $\pm$ 0.023 (6)
D_{MCL} TPZ	cm^{2}s^{-1} $\times$ 10^6	Diffusion coefficient of TPZ in HT29 MCL	0.40 $\pm$ 0.01 (12)
ϕ_c		Intracellular volume fraction (calculated)	0.517 $\pm$ 0.017 (20)
ϕ_e		Intracellular volume fraction (experimental)	0.508 $\pm$ 0.040 (6)

HT29 cells dissociated enzymatically from MCLs (1.23 pl[4]). Using this measured cell volume, we then estimated the intracellular volume fraction in MCLs (ϕ_c) needed to account for the transport impediment in anoxic MCLs by fitting the anoxic MCL flux data using the oxic D_{MCL} and the single cell metabolism model. The fitted value of ϕ_c showed no significant trend with concentration (Fig. 6*B*), provided that both the Michaelis Menten and first order terms were included. We then asked whether the average value of ϕ_c corresponds to the actual cell volume fraction in intact MCLs by measuring the latter directly, again using the $[^3H]_2O/[^{14}C]$mannitol method. The measured MCL intracellular volume fraction, ϕ_e, was indeed in good agreement with ϕ_c (Table 1). The concentration independence of ϕ_c, and its agreement with ϕ_e, demonstrates that the metabolism model in single cells provides an excellent description of TPZ metabolism at the tissue-like cell densities in MCLs.

TPZ Cytotoxicity in HT29 MCLs. Cell killing was quantified by exposing anoxic MCLs to TPZ at up to 100 μM for 1 or 2 h, with the drug added to both sides of the MCLs, then dissociating with trypsin to determine clonogenic survival. Cytotoxicity was greatly reduced relative to exposure of single cell suspensions under equivalent conditions, as shown in Fig. 7*A*. This ignores any difference in actual TPZ concentrations in the cells as a result of compromised transport into anoxic MCLs. To test whether the transport problem quantitatively accounts for the apparent resistance in MCLs, we calculated the expected killing using the PK (transport) and PD (cytotoxicity) parameters determined above. For each MCL, the effective thickness was determined from the urea flux (before the addition of TPZ), and TPZ concentration-time profile and cell killing was calculated as a function of distance from the MCL surface as shown for a representative MCL in Fig. 7*B*. Spatially averaging across this MCL gave a predicted mean surviving fraction of 0.20, whereas a value of 0.002 would be expected in single cell culture under the same exposure conditions. The measured surviving fraction for this MCL was 0.23. Across the 23 MCLs investigated, the predicted surviving fractions were in good agreement with measured cell killing (Fig. 7*C*).

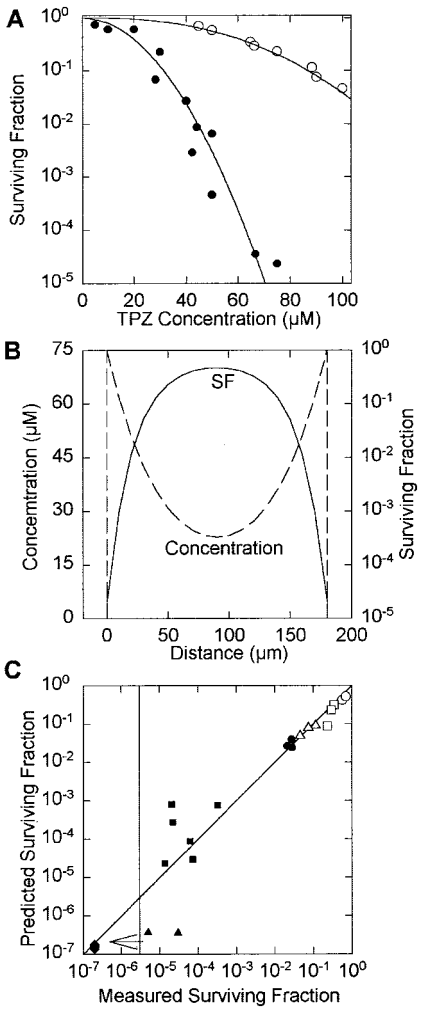

Fig. 7. Multicellular resistance of HT29 cells to TPZ in anoxic MCLs, and its relationship to TPZ transport. *A*, clonogenic survival curves for single cell suspensions (●) and intact MCLs (○) after exposure to TPZ for 1 h. *B*, simulation of the steady-state TPZ concentration profile 10 min after the addition of drug to both sides of a MCL, with thickness at 181 μm as measured by urea diffusion (*dashed line*) and surviving fraction predicted by the PK/PD model after 1-h exposure (*solid line*). *C*, correlation between predicted and measured mean surviving fractions in all MCL cytotoxicity experiments, in which MCLs were exposed to 50 μM TPZ (○, ●), 75 μM TPZ (□, ■), or 100 μM TPZ (△, ▲) for 1 h (*open symbols*) or 2 h (*closed symbols*). The *arrow* indicates predicted surviving fractions below the sensitivity limit of the assay (*vertical line*) for four MCLs exposed to 100 μM TPZ for 2 h (no colonies observed). These points were not included in the regression analysis.

DISCUSSION

This study demonstrates that anoxic HT29 cells in three-dimensional MCLs are resistant to TPZ, relative to anoxic single cells obtained from the same MCLs by a brief trypsinization (Fig. 7*A*). To assess the extent to which this multicellular resistance is caused by failure of TPZ to penetrate anoxic MCLs, we have measured the transport of TPZ through HT29 MCLs. This provided a mathematical model of TPZ transport that has allowed us to calculate the concentration-time profile as a function of distance into MCLs (Fig. 7*B*). We have also developed a PK/PD model that relates cell killing to TPZ exposure, and to its metabolic activation, in isolated HT29 cells. Combining the PK/PD model for cell suspensions with the MCL transport model has enabled us to predict cell killing as a function of position in MCLs (Fig. 7*B*). Averaging this calculated surviving fraction over the whole MCL provided predicted values in good agreement with the measured (average) surviving fraction (Fig. 7*C*).

The success of this spatially resolved PK/PD model indicates that there is no need to invoke any mechanism other than drug penetration limitations to account for the apparent resistance of cells in multicellular structures to TPZ. The corollary of this is that the intrinsic sensitivity of HT29 cells to TPZ is the same whether these cells are exposed in intact MCLs or as single cells, at least when the cells are exposed to the drug promptly after their isolation from MCLs. This has implications for the development of new analogues of TPZ, suggesting that critical elements of the overall PK/PD model such as rates of anoxic metabolism and cytotoxic potency can be determined meaningfully using single cell suspensions. We are currently using this approach, in conjunction with measurement of penetration through MCLs and the oxygen dependence of metabolism and cytotoxicity, to model response in HT29 tumors, and have recently demonstrated that this has strong predictive value (unpublished data).

The finding that extravascular transport limitations account for resistance of MCL cultures to TPZ does not necessarily preclude the existence of other forms of multicellular resistance if these persist for several hours after enzymatic dissociation of the three-dimensional structures. The "contact effect," first demonstrated by the resistance of cells in small spheroids to ionizing radiation (1), is known to show such persistence (4, 6). Similarly, resistance because of cytokinetic changes in MCLs, or to other relatively slow changes in gene expres-

[4] There was a significant ($P < 0.01$) difference in cell volume between anoxic (0% O_2) cell suspensions (1.40 ± 0.02 pl; $n = 12$) and hyperoxic (95% O_2) cell suspensions (1.09 ± 0.06 pl; $n = 16$). For purposes of scaling the intracellular volume fraction from cell suspensions to MCLs, the pooled average of these values has been used.

sion, cannot be expected to reverse quickly after trypsinization of MCLs or spheroids. Whether there are subsequent changes in sensitivity as cells adapt to growth as log-phase monolayers is not addressed by this study, but we see it is an advantage that the PK/PD model approach described here does not require use of monolayers that potentially introduce artifacts in chemosensitivity testing (5, 6, 13). Given that TPZ has been shown to act as a hypoxia-selective TopoIIα poison (28), and that cells in three-dimensional contact can be resistant to TopoII poisons relative to monolayers because of changes in TopoII phosphorylation and nuclear accumulation (29), differences in TPZ sensitivity might well be expected between monolayers and cells in MCLs or tumors. Changes in sensitivity to apoptosis via cell contact (5) could also contribute and might become important in modeling tumor response if cell contact after TPZ exposure suppressed apoptotic cell killing.

Determination of the parameters of the PK/PD model for HT29 cells, as required for this study, has also strengthened understanding of key steps in the mechanism of action of TPZ. The anoxic cytotoxicity of TPZ against HT29 single cell suspensions is in good agreement with an independent study showing similar cell kill after 1-h exposure of HT29 cell suspensions (30). The approximate quadratic dependence on concentration seen with HT29 cells is a general finding across cell lines (30, 31). We show (see "Appendix I") that the observed dependence of killing on $C^2 \times T$ at low cell density is consistent with the proposed "dual action" of TPZ cytotoxicity (32, 33). In this model, the rate of killing is proportional to the rate of metabolism of TPZ to a DNA-oxidizing radical (shown as TPZ* in Fig. 1) and to the TPZ concentration. The latter is consistent with the proposed second step in the action of TPZ in which it oxidizes the initial DNA radicals to generate DNA strand breaks, shown as step 2 in Fig. 1. The importance of the first step is consistent with other studies that have demonstrated a strong correlation between the rate of TPZ metabolism and cytotoxicity in several cell lines (30, 31).

The detailed investigation of TPZ metabolism in HT29 cells extends previous studies with cell lysates and isolated enzymes (34, 35) and cell suspensions (30, 31, 36, 37), the latter study reporting first order metabolism in HT29 cells at rates comparable with the present study. The previous studies did not detect saturable metabolism of TPZ at low concentrations, but the presence of two kinetic components was clearly evident over the wide concentration range investigated in this study. The kinetic data do not define the K_m of this component with precision (Table 1), but the saturable reductase(s) are important at concentrations <10 μM, which makes them significant in anoxic MCLs when the input TPZ concentration is ≤ 25 μM. We also predict that the Michaelis-Menten kinetic component will be important *in vivo*, because PK/PD modeling indicates that much of the exposure in hypoxic regions is at concentrations below 10 μM.[5] The nonsaturable first order component may be largely attributable to reduction by cytochrome P450 reductase, which is a promiscuous electron donor in the endoplasmic reticulum (38) and is probably the quantitatively major TPZ reductase (39, 40). It is tempting to speculate that the saturable component is caused by the TPZ reductase(s) in the nuclear matrix, which is considered to make a disproportionate contribution to TPZ cytotoxicity (41). However, there is no indication from our PK/PD modeling that the saturable component makes a larger contribution to cell killing.

This study further extends the use of the MCL model for cytotoxicity (PD) studies, in which the effective thickness of the tissue can be measured accurately by the flux of a tracer (*e.g.*, urea) during the experiment. To achieve the level of accuracy required for this study, precise measurement of MCL thickness and medium TPZ concentrations was essential because small differences in the penetration distance or initial drug concentration can lead to large differences in the average cell kill. The present validation of MCLs as an experimental model for quantifying TPZ transport, and the spatially resolved PK/PD model for cytotoxicity in MCLs, supports the use of these tools for developing an analogue of TPZ in which extravascular transport limitations are minimized. More generally, the present study points to a methodology with considerable potential for assisting lead optimization in anticancer drug development by providing information on PK as a function of distance from blood vessels in tumors. Thus, *in vitro* studies with multicellular layers have the potential to not only elucidate the relative importance of transport limitations in multicellular resistance but also to introduce transport considerations in the early stages of drug design. This PK/PD model is currently being extended by incorporating the O_2 dependence of TPZ metabolism and cytotoxicity, and by applying it to three-dimensional diffusion in tumor microvascular networks.

ACKNOWLEDGMENTS

The technical assistance of Dianne Ferry and Hui Hui Phua for single cell metabolism studies and Lorraine Rolston and Andrew Maslin for MCL histology is gratefully acknowledged.

APPENDIX

Appendix I. PK/PD Model for TPZ Metabolism and Cytotoxicity in Single Cell Suspensions. Because TPZ is metabolized only within cells in anoxic cultures (see "Results"), the cumulative amount metabolized per unit of intracellular volume (M) is

$$M(t) = ([TPZ]_0 - [TPZ])/\phi \tag{A1}$$

where ϕ is the intracellular volume fraction determined from the cell density (Coulter count) and cell volume, $[TPZ]$ is the concentration of TPZ averaged over the whole culture volume at time t, and $[TPZ]_0$ is the corresponding initial TPZ concentration. Given the low cellular uptake factor for TPZ (see "Results"), $[TPZ]$ is well approximated by the extracellular concentration at low values of ϕ. Anoxic TPZ metabolism in stirred single cell suspensions had both a first order and saturable (Michaelis-Menten) component over the concentration range examined; thus

$$\frac{dM}{dt} = -\frac{1}{\phi}\frac{d[TPZ]}{dt} = \left(k_{met}[TPZ] + \frac{V_{max}[TPZ]}{K_m + [TPZ]}\right) \tag{A2}$$

where k_{met} is the first order metabolic rate constant, V_{max} is the maximal rate of Michaelis-Menten metabolism, and K_m is the Michaelis constant. SR 4317 production was proportional TPZ metabolized, thus:

$$[\text{SR4317}] = \phi f_m M(t) \tag{A3}$$

where f_m is the stoichiometric relationship (fraction of TPZ lost that appears as SR 4317). The PD relationship between TPZ, metabolism, and cytotoxicity was described well (Fig. 4) by an empirical model in which the rate of fall in the log-surviving fraction (SF) was proportional to the rate of its bioreductive metabolism and to the TPZ concentration:

$$-\frac{d \log SF}{dt} = \alpha[TPZ]\frac{dM}{dt} \tag{A4}$$

where α is a proportionality constant. The data fit was improved by including a lag period, T_{lag}, in which there was no cell killing:

$$-\log SF = 0, \quad t \leq T_{lag}. \tag{A5}$$

[5] F. B. Pruijn, J. R. Sturman, H. D. S. Liyanage, K. O. Hicks, M. P. Hay, and W. R. Wilson, Extravascular transport of drugs in tumor tissue: effect of lipophilicity on diffusion of tirapazamine analogs in multicellular layer cultures, submitted for publication.

The value of T_{lag} was found to vary between experiments (coefficient of variation, 21.2%; range, 7.3–24.1 min), possibly because of oxygen contamination at zero time, whereas the coefficient α gave more consistent values (coefficient of variation, 2.0%). All equations were solved numerically using a fourth order Runge-Kutta method in Modelmaker version 4.0 (Cherwell Scientific Ltd., Oxford, UK), fitting all [TPZ], [SR4317], and *SF* data simultaneously by nonlinear least squares regression. Note that in the limiting case of low cell density, $[TPZ] \cong [TPZ]_0$, the predicted amount of metabolism is approximately

$$M(t) \cong R_0[TPZ]_0 \times t \tag{A6}$$

where

$$R_0 = \left(k_{met} + \frac{V_{max}}{K_m + [TPZ]_0} \right) \tag{A7}$$

and, thus, the PD model takes the form

$$-\log SF = \alpha R_0[TPZ]_0^2 \times (t - T_{lag}). \tag{A8}$$

This allowed initial parameter estimates by linear regression of log *SF versus* time for each curve. The intersection at log $SF = 0$ gave an estimate of T_{lag} in each experiment. Replotting log *SF* against $[TPZ]_0 \times (M(t)–M(T_{lag}))$ allowed estimation of α by linear regression for each experiment.

Appendix II. PK Model for TPZ Transport in MCLs. Transport was modeled as a one-dimensional diffusion through the MCL, in series with the collagen-coated Teflon support membrane as described previously (20, 25). For TPZ in the MCL, a reaction term is included to represent loss of drug attributable to metabolism:

$$\frac{\partial[TPZ]}{\partial t} = D \frac{\partial^2[TPZ]}{\partial x^2} - \phi \frac{\partial M}{\partial t} \tag{A9}$$

and

$$\frac{\partial M}{\partial t} = \left(k_{met}[TPZ] + \frac{V_{max}[TPZ]}{K_m + [TPZ]} \right) \tag{A10}$$

where D is the diffusion coefficient of *TPZ* and the other parameters are as "Appendix I," except that M is now a function of distance x as well as t. The far end boundary conditions were for zero flux in the donor and receiver compartments with diffusion occurring only through the MCL. The initial conditions set [*TPZ*] to its initial measured concentration in the donor compartment and to 0 elsewhere. Analogous equations, without a metabolism term, were used to model the concentrations of the internal standard (urea). The transport model was solved numerically for the concentrations in the donor and receiver compartments simultaneously using the NAG Fortran Library Mark 19 routine, D03PCF, and fitted to the data by minimization of the residual sum of squares, with compensation for volume removed during sampling as described previously (24) and for evaporative concentration (estimated from the urea mass balance). Calculations were performed on an Intel Pentium III computer using the Digital Visual Fortran version 6.0 implementation of the Fortran 77 programming language.

REFERENCES

1. Durand, R. E., and Sutherland, R. M. Effects of intercellular contact on repair of radiation damage. Exp. Cell Res., *71:* 75–80, 1972.
2. Teicher, B. A., Herman, T. S., Holden, S. A., Wang, Y. Y., Pfeffer, M. R., Crawford, J. W., and Frei, E., III. Tumor resistance to alkylating agents conferred by mechanisms operative only in vivo. Science (Wash. DC), *247:* 1457–1461, 1990.
3. Kobayashi, H., Man, S., Graham, C. H., Kapitain, S. J., Teicher, B. A., and Kerbel, R. S. Acquired multicellular-mediated resistance to alkylating agents in cancer. Proc. Natl. Acad. Sci. USA, *90:* 3294–3298, 1993.
4. Olive, P. L., and Durand, R. E. Drug and radiation resistance in spheroids: cell contact and kinetics. Cancer Metastisis Rev., *13:* 121–138, 1994.
5. Green, S. K., Frankel, A., and Kerbel, R. S. Adhesion-dependent multicellular drug resistance. Anticancer Drug Des., *14:* 153–168, 1999.
6. Durand, R. E., and Olive, P. L. Resistance of tumor cells to chemo- and radiotherapy modulated by the three-dimensional architecture of solid tumors and spheroids. Methods Cell Biol., *64:* 211–233, 2001.
7. St. Croix, B., Florenes, V. A., Rak, J. W., Flanagan, M., Bhattacharya, N., Slingerland, J. M., and Kerbel, R. S. Impact of the cyclin-dependent kinase inhibitor p27Kip1 on resistance of tumor cells to anticancer agents. Nat. Med., *2:* 1204–1210, 1996.
8. St. Croix, B., Sheehan, C., Rak, J. W., Florenes, V. A., Slingerland, J. M., and Kerbel, R. S. E-cadherin-dependent growth suppression is mediated by the cyclin- dependent kinase inhibitor p27(KIP1). J. Cell Biol., *142:* 557–571, 1998.
9. Kantak, S. S., and Kramer, R. H. E-cadherin regulates anchorage-independent growth and survival in oral squamous cell carcinoma cells. J. Biol. Chem., *273:* 16953–16961, 1998.
10. Hague, A., Hicks, D. J., Bracey, T. S., and Paraskeva, C. Cell-cell contact and specific cytokines inhibit apoptosis of colonic epithelial cells: growth factors protect against c-myc-independent apoptosis. Br. J. Cancer, *75:* 960–968, 1997.
11. Durand, R. E. The influence of microenvironmental factors during cancer therapy. In Vivo (Athens), *8:* 691–702, 1994.
12. Wartenberg, M., Frey, C., Diedershagen, H., Ritgen, J., Hescheler, J., and Sauer, H. Development of an intrinsic P-glycoprotein-mediated doxorubicin resistance in quiescent cell layers of large, multicellular prostate tumor spheroids. Int. J. Cancer, *75:* 855–63, 1998.
13. Tannock, I. F. Tumor physiology and drug resistance. Cancer Metastisis Rev., *20:* 123–132, 2001.
14. Durand, R. E. Intermittent blood flow in solid tumours–an under-appreciated source of 'drug resistance.' Cancer Metastisis Rev., *20:* 57–61, 2001.
15. Brown, J. M., and Giaccia, A. J. The unique physiology of solid tumors: opportunities (and problems) for cancer therapy. Cancer Res., *58:* 1408–1416, 1998.
16. Zeman, E. M., Brown, J. M., Lemmon, M. J., Hirst, V. K., and Lee, W. W. SR-4233: a new bioreductive agent with high selective toxicity for hypoxic mammalian cells. Int. J. Radiat. Oncol. Biol. Phys., *12:* 1239–1242, 1986.
17. Brown, J. M. SR 4233 (tirapazamine): a new anticancer drug exploiting hypoxia in solid tumours. Br. J. Cancer, *67:* 1163–1170, 1993.
18. Denny, W. A., and Wilson, W. R. Tirapazamine: a bioreductive anticancer drug that exploits tumour hypoxia. Expert Opin. Investig. Drugs, *9:* 2889–2901, 2000.
19. Durand, R. E., and Olive, P. L. Evaluation of bioreductive drugs in multicell spheroids. Int. J. Radiat. Oncol. Biol. Phys., *22:* 689–692, 1992.
20. Hicks, K. O., Fleming, Y., Siim, B. G., Koch, C. J., and Wilson, W. R. Extravascular diffusion of tirapazamine: effect of metabolic consumption assessed using the multicellular layer model. Int. J. Radiat. Oncol. Biol. Phys., *42:* 641–649, 1998.
21. Phillips, R. M., Loadman, P. M., and Cronin, B. P. Evaluation of a novel in vitro assay for assessing drug penetration into avascular regions of tumours. Br. J. Cancer, *77:* 2112–2119, 1998.
22. Kyle, A. H., and Minchinton, A. I. Measurement of delivery and metabolism of tirapazamine to tumour tissue using the multilayered cell culture model. Cancer Chemother. Pharmacol., *43:* 213–220, 1999.
23. Mason, J. C., and Tennant, G. Heterocyclic N-oxides. Part VI. Synthesis and nuclear magnetic resonance spectra of 3-aminobenzo-1, 2, 4-triazines and their mono- and di-N-oxides. J. Chem. Soc. (B), 911–916, 1970.
24. Hicks, K. O., Ohms, S. J., van Zijl, P. L., Denny, W. A., Hunter, P. J., and Wilson, W. R. An experimental and mathematical model for the extravascular transport of a DNA intercalator in tumours. Br. J. Cancer, *76:* 894–903, 1997.
25. Hicks, K. O., Pruijn, F. B., Baguley, B. C., and Wilson, W. R. Extravascular transport of the DNA intercalator and topoisomerase poison *N*-[2-(dimethylamino)ethyl]acridine-4-carboxamide (DACA): diffusion and metabolism in multicellular layers of tumor cells. J. Pharmacol. Exp. Ther., *297:* 1088–1098, 2001.
26. Wilson, W. R., Pullen, S. M., Hogg, A., Hobbs, S. M., Pruijn, F. B., and Hicks, K. O. In vitro and in vivo models for evaluation of GDEPT: quantifying bystander killing in cell cultures and tumors. *In:* C. J. Springer (ed.), Suicide Gene Therapy: Methods and Protocols for Cancer. Totowa, NJ: Humana Press, in press, 2003.
27. Ferry, D. M., van Zijl, P. L., and Wilson, W. R. Sensitive liquid chromatographic assay for the basic DNA intercalator (*N*,*N*-dimethylaminoethyl)-9-amino-5-methylacridine-4-carboxamide and its nitroarylmethyl quaternary prodrugs in biological samples. J. Chromatogr. B Biomed. Sci. Appl., *763:* 149–156, 2001.
28. Peters, K. B., and Brown, J. M. Tirapazamine: a hypoxia-activated topoisomerase II poison. Cancer Res., *62:* 5248–5253, 2002.
29. Oloumi, A., MacPhail, S. H., Johnston, P. J., Banath, J. P., and Olive, P. L. Changes in subcellular distribution of topoisomerase IIα correlate with etoposide resistance in multicell spheroids and xenograft tumors. Cancer Res., *60:* 5747–5753, 2000.
30. Siim, B. G., van Zijl, P. L., and Brown, J. M. Tirapazamine-induced DNA damage measured using the comet assay correlates with cytotoxicity towards hypoxic tumour cells *in vitro*. Br. J. Cancer, *73:* 952–960, 1996.
31. Biedermann, K. A., Wang, J., Graham, R. P., and Brown, J. M. SR 4233 cytotoxicity and metabolism in DNA repair-competent and repair- deficient cell cultures. Br. J. Cancer, *63:* 358–362, 1991.
32. Jones, G. D., and Weinfeld, M. Dual action of tirapazamine in the induction of DNA strand breaks. Cancer Res., *56:* 1584–1590, 1996.
33. Hwang, J. T., Greenberg, M. M., Fuchs, T., and Gates, K. S. Reaction of the hypoxia-selective antitumor agent tirapazamine with a C1′-radical in single-stranded and double-stranded DNA: the drug and its metabolites can serve as surrogates for molecular oxygen in radical- mediated DNA damage reactions. Biochemistry, *38:* 14248–14255, 1999.
34. Wang, J., Biedermann, K. A., Wolf, C. R., and Brown, J. M. Metabolism of the bioreductive cytotoxin SR 4233 by tumour cells: enzymatic studies. Br. J. Cancer, *67:* 321–325, 1993.
35. Patterson, A. V., Barham, H. M., Chinje, E. C., Adams, G. E., Harris, A. L., and Stratford, I. J. Importance of P450 reductase activity in determining sensitivity of breast tumour cells to the bioreductive drug, tirapazamine (SR 4233). Br. J. Cancer, *72:* 1144–1150, 1995.

36. Baker, M. A., Zeman, E. M., Hirst, V. K., and Brown, J. M. Metabolism of SR 4233 by Chinese hamster ovary cells: basis of selective hypoxic cytotoxicity. Cancer Res., *48:* 5947–5952, 1988.
37. Giaccia, A. J., Biedermann, K. A., Tosto, L. M., Minchinton, A. I., Kovacs, M. S., and Brown, J. M. Characterization of a CHO cell line resistant to killing by the hypoxic cell cytotoxin SR 4233. Int. J. Radiat. Oncol. Biol. Phys., *22:* 681–684, 1992.
38. Butler, J., and Hoey, B. M. The one-electron reduction potential of several substrates can be related to their reduction rates by cytochrome P-450 reductase. Biochim. Biophys. Acta, *1161:* 73–78, 1993.
39. Fitzsimmons, S. A., Lewis, A. D., Riley, R. J., and Workman, P. Reduction of 3-amino-1,2,4-benzotriazine-1,4-di-N-oxide (tirapazamine, WIN 59075, SR 4233) to a DNA-damaging species: a direct role for NADPH:cytochrome P450 oxidoreductase. Carcinogenesis (Lond.), *15:* 1503–1510, 1994.
40. Patterson, A. V., Saunders, M. P., Chinje, E. C., Talbot, D. C., Harris, A. L., and Stratford, I. J. Overexpression of human NADPH:cytochrome c (P450) reductase confers enhanced sensitivity to both tirapazamine (SR 4233) and RSU 1069. Br. J. Cancer, *76:* 1338–1347, 1997.
41. Evans, J. W., Yudoh, K., Delahoussaye, Y. M., and Brown, J. M. Tirapazamine is metabolized to its DNA-damaging radical by intranuclear enzymes. Cancer Res., *58:* 2098–2101, 1998.
42. Daniels, J. S., and Gates, K. S. DNA cleavage by the antitumor agent 3-amino-1,2,4-benzotriazine 1,4-dioxide (SR4233): evidence for involvement of hydroxyl radical. J. Am. Chem. Soc., *118:* 3380–3385, 1996.
43. Anderson, R. F., Shinde, S. S., Hay, M. P., Gamage, S. A., and Denny, W. A. Activation of 3-amino-1,2,4-benzotriazine 1,4-dioxide antitumor agents to oxidizing species following their one-electron reduction. J. Am. Chem. Soc., *125:* 748–756, 2003.

Multicellular Resistance to Tirapazamine Is Due to Restricted Extravascular Transport: A Pharmacokinetic/Pharmacodynamic Study in HT29 Multicellular Layer Cultures

Kevin O. Hicks, Frederik B. Pruijn, Joanna R. Sturman, et al.

Cancer Res 2003;63:5970-5977.